3-D Catalytic Regeneration Modeling of SiC Diesel Particulate Filters

George Pontikakis and Anastassios Stamatelos[1]
Mechanical & Industrial Engineering Department,
University of Thessaly, 383 34 Volos, Greece

Abstract

Increasingly stringent diesel particulate emissions standards have re-established international interest in Diesel filters, whose first series application dates back to 1985. Modern Diesel engine technology, with computerized engine management systems and advanced, common rail injection systems, needs to be fully exploited to support efficient and durable Diesel filter systems with catalytic aids, as standard equipment in passenger cars. Efficient system and components' optimization requires the use of mathematical models of Diesel filter performance. The three-dimensional model for the regeneration of the diesel particulate filter presented in this paper, has been developed as an engineering tool for the detailed design optimization of SiC Diesel filters of modular structure. The 3-D modeling is achieved by interfacing an existing 1-D model to commercial FEM software for the computation of the 3D temperature field within the whole filter assembly, including the adhesive of the filter blocks, the insulation mat and the metal canning. The 3-D model is applied to real-world component optimization studies of Diesel filter systems.

[1] Corresponding author: Tel. +30 24210 74067, Fax. +30 24210 74096, Email: stam@uth.gr

1 Introduction

Cellular ceramic diesel particulate filters with catalytic assistance have demonstrated the capacity to attain the extremely stringent particulate matter emissions of EPA Tier II and EURO 4 – EURO 5 standards, both for passenger cars and for Heavy Duty Vehicles. Diesel filter applications date back to the 1980's. Nevertheless, their series application was not realized until recently, because of problems regarding filter reliability and durability, which were associated with the regeneration of the filter. During regeneration, the accumulated particulate matter (also referred-to as soot) is oxidized to CO_2 and CO. The soot oxidation reactions are followed by significant heat release, which may endanger the integrity of the filter under certain operating conditions. A typical scenario of filter regeneration that may lead to filter damage is illustrated in Figure 1. A sudden deceleration of the vehicle occurring shortly after the onset of regeneration in a heavily loaded SiC Diesel Filter results in high oxygen concentration and low mass flow rates in the filter inlet gas stream. This leads to uncontrolled filter regeneration and excessive heat release that causes temperatures at the center of the filter to rise to about 900°C (even higher, locally). In addition to the advantageous higher thermal conductivity, compared to Cordierite, SiC has a higher melting point, which adds to its durability. On the other hand, SiC has a higher thermal expansion coefficient, thus it is more prone to thermal stresses due to temperature gradients within the filter. SiC filters are usually made up of smaller filter blocks, which are glued together with adhesive cement. The adhesive normally has a lower thermal conductivity than SiC, a fact that inhibits conduction in the radial direction. SiC filters are increasingly employed in passenger cars, coupled with catalytic regeneration techniques (catalytic fuel additives or washcoated filters) [1]. The capabilities of modern Diesel engine management and injection systems (post injection) are employed to increase exhaust gas temperature to achieve the onset of regeneration. Thus, the Diesel filter forms the core device of an integrated system. The need for engineering modeling tools has thus emerged [2,3] to assist Diesel filter and overall exhaust system design optimization.

Out of a variety of modeling approaches available, the final selection depends on the nature of the design problem posed to the engineer. Most prominent factors, though, should be the following:

- level of optimization detail
- data availability
- computational cost and cost of use
- model consistency and reliability

The level of optimization detail that the engineer pursues greatly influences the complexity of the model itself. For relatively simple or preliminary design and optimization, simpler models are preferred to more complicated ones. Difficulty in model development and validation grows rapidly with increase of model complexity, a fact that might create uncertainty about the reliability of highly complex models results. Furthermore, sophisticated models with many degrees of freedom also require detailed input data such as exhaust gas velocity profiles or complex reaction kinetics. More

often than not, such data are not routinely available. More sophisticated models also require higher expertise from the user, higher computational cost, and are more labour intensive in their results post-processing and conclusions drawing.

Having the above in mind, we present in this paper a 3-D model for the regeneration of the diesel particulate filter, to be employed as a tool for the detailed optimization of the structure and geometry of SiC Diesel filters of modular structure. The model is incorporated in an integrated methodology for the computer-aided engineering of the total exhaust treatment system, which also comprises pre- and post-processing procedures, code validation with design and quality assurance of supporting experiments and tests, model tuning procedure and application in the design and optimization of target exhaust treatment systems.

The 3-D model described in this work is based on the CATWALL 1-D model, which has been extensively validated in the past [10, 11, 24]. It may be used either via the MATLAB/Simulink environment, or as a stand-alone tool, supported by a set of Excel macros for pre- and post-processing of data. The extension of the model to three dimensions is obtained by linking it to commercial FEM software for the computation of the 3-D temperature field within the whole filter assembly, including the adhesive of the filter blocks, the insulation mat and the metal canning. The feasibility of this approach had been investigated previously [4]. The model incorporates a module for the computation of non-uniform flow distribution caused by non-uniform soot deposit of the different channels.

2 Modeling catalytic regeneration

2.1 General

Chemical phenomena in Diesel filter regeneration include (a) the combustion of the soot layer because of thermal and catalytic reactions and (b) the adsorption, desorption and combustion of hydrocarbons contained in the soot particles (Volatile Organic Fraction). The primary physical phenomena of the filter operation are (a) the heat transfer in the filter and (b) the distribution of the flow field, which is affected by the distribution of the soot layer within the filter.

The first attempt to provide a mathematical description of the regeneration process of the soot layer was the pioneering work of Bissett [5]. Their first model was a zero-dimensional regeneration model. It was concerned with thermal soot combustion in one point of a filter channel, and flow and soot distribution within the channels of the filter was averaged. Despite its apparent simplicity, this work has been remarkable in that it essentially defined a robust mathematical framework for the description of the physical and chemical phenomena in the soot layer and filter wall, and some significant simplifying assumptions were established. The initial model was later extended to 1-D, also accounting for the axial heat conduction and the soot layer and flow distribution along the channel [6].

This work has been adopted and extended in [7], allowing the study and experimental validation of high space velocity thermal regeneration events, with a systematic methodology of filter loading assessment by energy balances. It was further extended to cover catalytic regeneration, in zero-

dimensions [8], and also in 1-D [9], while further refinements and improvements of the regeneration model were validated by extensive experimental data [10,11,12].

As regards the basic assumptions, and if we take out the chemical reactions submodel, the majority of the models in use today could be considered as extensions of [5,6]. Minor improvements have been presented, as the raising of the uniform soot and wall temperature across the wall [13]. A number of studies has been done focusing to the extension to 2D [14,15,16]. However, the reaction scheme remained very simplified in all cases, (thermal Carbon oxidation, in spite of the fact that all diesel filter systems in use today are based on the use of catalysts) and extensive validation of a 2-D model was only presented in [15].

Since the regeneration process in the filter is essentially three-dimensional, especially at low flowrates, and significant flow and soot maldistribution is reported [17], which may also result in partial burning of the soot [18], a further extension of the above model has been attempted for the 3-D modeling of the heat conduction within the filter by linking the channel model [9] with commercial finite element software. In this work, we apply this concept to build a 3-D model for the regeneration process in the filter by interfacing the 1-D model with the ANSYS [19] finite element software package. The 1-D model features an inclusive reaction scheme for the thermal and catalytic regeneration of the soot. Analytical solutions of the pertinent balance equations are obtained, including an updated catalytic regeneration reactions scheme and a more detailed view of the soot layer geometry. Finally, the model is enhanced with a module to account for flow maldistribution at the filter inlet because of non-uniform soot loading of the filter, which is usually a result of incomplete filter regeneration.

It should be noted that the reaction rates that have been used in all filter regeneration models are essentially of the Arrhenius-type, i.e. the rates are analogous to the factor $k = A\exp\left(-E/R_gT\right)$. This implies that the activation energy E and the pre-exponential factor A must be determined for each reaction involved in the reaction scheme.

2.2 Geometry of the channels and the soot layer

The filter consists of a ceramic grid of parallel channels. Adjacent channels are alternatively plugged at each end in order to force the diesel aerosol through the porous walls. Thus, diesel particulate matter is deposited on the four sides of each inlet channel. Because of the repeating geometry of the filter, one may restrict the mathematical treatment to a unit computational cell as seen in Figure 2. This fundamental volume consists of one inlet channel and four quarters of the four adjacent outlet channels. The boundaries of the volume are assumed adiabatic and no flow occurs through them to the rest of the outlet channel. From the standpoint of modeling, the whole filter is constructed by repeating this fundamental volume.

To formulate the balance equations pertinent for regeneration modeling, we consider a small part of this fundamental volume, of length Δz. At this part of the channel, a layer of soot of mass m and thickness w has already accumulated. The wall's thickness is w_s and the length of the channel edge

is ℓ . Exhaust gas flow is perpendicular to the soot layer and wall. Exhaust gas species are consumed or produced as gas flows through the soot layer. In this work, we shall use the subscript *p* to denote the physical properties of the soot layer and *s* to denote the corresponding properties of the wall.

It is evident from Figure 3 that the soot layer consists of four trapezoids. Assuming that some soot mass m_p of density ρ_p is deposited on a square filter channel with inner side length ℓ , the deposit thickness can be calculated as:

$$w_p = \frac{1}{2}\left(\ell - \sqrt{\ell^2 - \frac{m_p}{\rho_p \Delta z}} \right) \tag{1}$$

This relation is employed in the computation of the evolution of deposit thickness in the different channels and different nodes of each channel. As a consequence of the trapezoid distribution of the soot layer, the area perpendicular to the flow $A(x)$ (i.e. the area that the flow `faces' at each x) is also changing along x:

$$A(x) = \begin{cases} 4(2x + \ell)\Delta z, & -w_p \le x \le 0 \\ 4\ell \Delta z, & 0 \le x \le w_s \end{cases} \tag{2}$$

The volume of the soot layer V_p may be readily calculated from the above relationship.

$$V_p = 4\Delta z \left(\ell - w_p \right) w_p \tag{3a}$$

while the volume of the substrate is

$$V_s = 4\Delta z \left(\ell + 0.5 w_s \right) w_s \tag{3b}$$

Notice that it is common in the literature to consider only one of the four sides of the channel instead of the computational cell of Figure 2. Such a simplification would also yield slightly simpler expressions for w_p, $A(x)$ and V_p, since the trapezoid shape of the soot layer would not be taken into account. In fact, this approach was adopted in earlier works, e.g. [5,6]. However, the total mass of the ceramic substrate and also the thickness of the soot layer w as a function of soot load would be incorrectly calculated, introducing some error in the thermal inertia and pressure drop calculation, respectively. Admittedly, these errors would not change the behavior of the model dramatically. Nevertheless, the extension described in Figure 2 and equations (1) – (3) was adopted because it does not complicate the model significantly.

2.3 Reaction kinetics

The soot that is deposited in the filter walls consists mainly of carbon and adsorbed hydrocarbons (VOF). When a fuel additive is used to assist regeneration, it takes part in the combustion process in the engine's cylinder and the formation of particulate matter. Therefore, soot particles deposited in the trap contain bonded metal oxide particles, which react with the soot carbon and VOF at lower temperatures compared to thermal regeneration.

The kinetic model employed herein accounts for thermal soot oxidation by oxygen and for catalytic soot oxidation by a Ce-based fuel additive, but it does not yet include the effect for the VOF. The reactions along with their respective rate expressions are given in Table 1. The reaction rates for all reactions are assumed to depend on temperature according to a first order Arrhenius-type expression.

For thermal oxidation modeling, two reactions are employed, accounting for the oxidation of carbon by exhaust gas oxygen to CO_2 and CO respectively. Both reactions are assumed to be proportional to the oxygen concentration y in the exhaust gas. The latter has a significant distribution along the soot layer thickness, since it is gradually depleted therein. For the catalytic oxidation of carbon, a model was first formulated in [8]. The implemented mechanism is only valid when the catalytic oxide that has two oxidation states, which is true for Ceria. The first step of the mechanism is oxidation of Ce_2O_3 by O_2 to produce CeO_2. The second step involves reaction of CeO_2 with soot carbon. Ceria returns from its 4- to its 3-valent state, while carbon monoxide is produced. The presence of the additive does not prevent direct oxidation of carbon by oxygen, if the temperature is sufficient for this reaction.

For the oxidation of Ce_2O_3 by the exhaust gas oxygen, the reaction rate is assumed proportional to the oxygen concentration y in the exhaust gas, similarly to the thermal oxidation of C. The reaction rates of C oxidation by CeO_2 are assumed proportional to the quantity ψ which represents the percentage of Ce being in its higher oxidation state (CeO_2):

$$\psi = \frac{\text{mol CeO}_2}{\text{mol Ce}} = \frac{\text{mol CeO}_2}{2 \times \text{mol Ce}_2\text{O}_3 + \text{mol CeO}_2} \tag{4}$$

An additional term ξ will also be needed in the next section, though it does not appear in the reaction rates. It defined as the concentration of catalyst in the soot layer and is a function of metal additive concentration in the fuel. It may be expressed as:

$$\xi = \frac{\text{mol Ce}}{\text{mol soot}} = \frac{2 \times \text{mol Ce}_2\text{O}_3 + \text{mol CeO}_2}{\text{mol C}} \tag{5}$$

As it is evident from Table 1, the quantity ψ plays a similar role for catalytic soot oxidation with the O_2 concentration y for thermal soot oxidation. It should be noted, though, that both ψ and ξ are viewed as averaged quantities along the soot layer thickness, contrary to y which is assumed to have a distribution. Averaging ξ is expected because Ce is uniformly distributed in the soot layer, since it is bonded with the soot particles during the fuel combustion process, contrary to O_2 which flows through the soot layer where it is gradually depleted. The rationale behind the averaging of ψ stems from the need to suppress the model's dimensions, in order to keep the feasibility of analytical integration of the balance equations along the x dimension.

2.4 Mass and heat balances in the soot layer and ceramic wall (regeneration submodel)

As gas flows through the soot layer, the oxygen is gradually depleted because of reaction with carbon and Ceria. An oxygen concentration profile is thus established through the soot layer, which is expressed by an oxygen mass balance:

$$\frac{\dot{m}_g}{A(x)}\frac{dy(x)}{dx} = -M_g\left(k_1 + 0.5k_2 + 0.5k_5(1-\psi)\right)y(x) \tag{6}$$

The above mass balance may be solved to get the oxygen concentration profile $y(x)$, for the initial condition $y(x=-w_p)=y_{in}$, provided that the temperature of the soot layer is considered constant in a direction perpendicular to the soot layer (which is justified in the discussion about temperature boundary conditions later in this section). This is a fundamental assumption that is supported by the original work of Bissett [5] (see also the boundary conditions below). The solution yields the total consumption of oxygen $\Delta y = y(x=-w_p) - y(x=0)$ through the soot layer:

$$\Delta y = y_{in}\left[1 - \exp\left(-\frac{M_g\left(k_1 + 0.5k_2 + 0.5k_5(1-\psi)\right)}{\dot{m}_g}V_p\right)\right] \tag{7}$$

The total consumption of oxygen may be used in order to calculate the rate of soot consumption because of both thermal oxidation with oxygen and catalytic oxidation with Ceria. Specifically, the mass balance for the soot mass consumption is:

$$\frac{\rho_p}{M_p}\frac{dV_p}{dt} = -\int_{-w_p}^{0}\left[\left(k_1 + 0.5k_2\right)y(x) + \left(k_3 + k_4\right)\psi\right]A(x)dx \tag{8}$$

or, splitting the integral:

$$\frac{\rho_p}{M_p}\frac{dV_p}{dt} = -\left(k_1 + 0.5k_2\right)\int_{-w_p}^{0} y(x)A(x)dx - \left(k_3 + k_4\right)\psi\int_{-w_p}^{0} A(x)dx \tag{9}$$

The first integral contained in the right hand side of the above equation may be calculated from the oxygen mass balance (6):

$$\int_{-w_p}^{0} y(x)A(x)dx = \frac{\dot{m}_g}{M_g\left(k_1 + 0.5k_2 + 0.5k_5(1-\psi)\right)}\Delta y \tag{10}$$

The second integral of the soot mass balance is the volume of the soot layer V_p. Substituting the above, we get the following rate of soot mass consumption:

$$\rho_p\frac{dV_p}{dt} = -\frac{M_p}{M_g}\frac{k_1 + 0.5k_2}{k_1 + 0.5k_2 + 0.5k_5(1-\psi)}\dot{m}_g\Delta y - M_p\left(k_3 + k_4\right)\psi V_p \tag{11}$$

A mass balance must also be formulated for ψ, which expresses the continuous transition of the catalytic additive between CeO_2 and Ce_2O_3 states. According to the CeO_2 mass balance, the rate of change depends on the additive oxidation and reduction reactions, i.e.:

$$\left(\int_{-w_p}^{0}\frac{\rho_p A(x)dx}{M_p}\right)\xi\frac{d\psi}{dt} = \int_{-w_p}^{0}\left[-\left(4k_3 + 2k_4\right)\psi + 2k_5 y(1-\psi)\right]A(x)dx \tag{12}$$

The above equation may be simplified and, with the substitution of (10), yields the total rate of change for ψ:

$$\xi \frac{d\psi}{dt} = -\frac{M_p}{\rho_p}\left(4k_3 + 2k_4\right)\psi + \frac{2k_5\left(1-\psi\right)}{k_1 + 0.5k_2 + k_5\left(1-\psi\right)} \frac{\dot{m}_g}{\rho_p V_p} \frac{M_p}{M_g} \Delta y \qquad (13)$$

The two mass balance equations for soot and Ceria should be solved for the following initial conditions: For $t = t_0$ we have $V_p = V_{p,0}$ and $\psi = \psi_0$.

To complete the model, a heat balance equation must be formulated. This expresses the accumulation of heat in the soot layer and the ceramic wall because of (a) heat generation by the chemical reactions, (b) heat conduction perpendicular to the soot layer and wall and (c) heat exchange between the gaseous and the solid phase. Denoting the temperature of the solid phase (particle layer or substrate) as *T*, and the temperature of the exhaust gas as T_g, we have the following balance equations for the solid phase:

$$\rho_j c_{p,j} A(x) \frac{\partial T}{\partial t} = -\dot{q}(x) A(x) + \frac{\partial}{\partial x}\left(A(x) \lambda_j \frac{\partial T}{\partial x} \right) - \dot{m}_g c_{p,g} \frac{\partial T_g}{\partial x}, j=p,s \qquad (14)$$

where the heat flux $\dot{q}(x)$ [J/(m^{3}s)] is defined as the sum of the products of the reaction rates r_n [mol/(m^{3}s)] as defined in Table 1 and the reaction enthalpies ΔH_n [J/mol]:

$$\dot{q}(x) = \begin{cases} \sum_{n=1}^{5} r_n \Delta H_n & \text{if } -w_p \le x \le 0 \\ 0 & \text{if } \quad 0 \le x \le w_s \end{cases}$$

(No reactions occur as the gas flows through the ceramic wall, thus $\dot{q}(x)$ is zero in that region.)

Except from the solid phase temperature *T*, the above heat balance also contains the gas temperature T_g, which, in principle, has a separate profile $T_g(x)$ along the solid phase. Instead of solving for the two coupled temperature profiles of *T(x)* and $T_g(x)$, Bissett and Shadmann proved that the gas temperature T_g adjusts to the solid temperature in a length scale several orders of magnitude smaller than the soot layer thickness. That is, $T_g = T$ everywhere except at $x = -w_p$.

At $x = -w_p$, and at $x = +w_s$, according to Bissett and Shadmann, we have the following boundary conditions:

$$\begin{aligned} &\text{At } x = -w_p && T_g = T_{g,in} \\ & && A\left(x = -w_p\right) \lambda_p \frac{\partial T}{\partial x} = \dot{m}_g c_{p,g} \left(T - T_g\right) \\ &\text{At } x = +w_s && \frac{\partial T}{\partial x} = 0 \end{aligned} \qquad (15)$$

Using the above boundary condition at $x = -w_p$, we may integrate the second term of the right-hand side of the heat balance to get:

$$\int_{-w_p}^{+w_s} \frac{\partial}{\partial x}\left(A(x)\lambda_j \frac{\partial T}{\partial x} \right) = \dot{m}_g c_{p,g}\left(T - T_{g,in}\right)$$

Thus, the boundary conditions at $x = -w_p$ imply that all the heat content of the gas is immediately exchanged with the solid phase.

Furthermore, in the same work, Bissett and Shadmann also show mathematically that the temperature of the solid phase may be considered uniform along *x*. This is a critical result, and we have already used it in the integrations of the mass balances, since we have silently considered the reaction rate coefficients *k* (which depend strongly on temperature) as constant along *x*. This result also further simplifies the heat balance, since we readily find that the third term of the right-hand side is zero, since *dT/dx = 0*.

Under these conditions, the heat balance (14) is integrated to yield the rate *dQ/dt* that heat is released (a) by chemical reactions and (b) by convection because of flow normal to the soot layer and wall.

$$\begin{aligned} &\frac{dQ}{dt} = \left(\rho_p c_{p,p} V_p + \rho_s c_{p,s} V_s\right) = \\ &= -\frac{\left(\Delta H_1 k_1 + \Delta H_2 k_2 + 0.5\Delta H_5 k_5 (1-\psi)\right)}{k_1 + 0.5k_2 + 0.5k_5(1-\psi)} \frac{\dot{m}_g}{M_g} \Delta y - \left(\Delta H_3 k_3 + \Delta H_4 k_4\right)\psi V_p + \dot{m}_g c_{p,g}\left(T - T_g^{in}\right) \end{aligned} \quad (16)$$

2.5 Pressure drop submodel

The total pressure drop across the particulate layer and the ceramic wall can be expressed as the sum of the porous ceramic substrate pressure drop and the soot layer pressure drop:

$$\Delta p = \Delta p_s + \Delta p_p \quad (17)$$

It is generally accepted [20] that pressure drop across the porous walls of the ceramic filters can be approximated by Darcy's law. According to this law, the total pressure drop due to flow through the ceramic wall and the soot layer can be approximated by the following simplified relation:

$$\Delta p = p_{in} - p_{out} = \frac{\mu u_w w_s}{k_s} + \frac{\mu u_w w_p}{k_p} \quad (18)$$

By using the concept of effective particulate layer thickness [21], the latter formula can be rewritten as follows:

$$\Delta p = p_{in} - p_{out} = \frac{\mu u_w w_s}{k_s} + \frac{\mu u_w m_p}{A_f (\rho k)_p} \quad (19)$$

where A_f is the mean filtration area. This formula allows, in principle, the backward approximate calculation of collected soot mass as function of measured filter backpressure at a certain engine and

filter loading operation point, once an approximate value for the product $(\rho k)_p$, that is, (soot layer density) times (soot layer permeability) is known for the specific engine – filter – operation point combination.

2.6 1-D modeling of the flow distribution and pressure losses in the channel

The above pressure drop and regeneration model is a zero-dimensional approach to filter modeling, in the sense that it is valid for each point z along the filter axis, but does not provide any information regarding axial profiles of temperature, pressure drop and mass distribution. This is accomplished below, employing the following balance equations: (i) the conservation of the exhaust gas mass flow, (ii) the conservation of the axial component of momentum of exhaust gas and (iii) the conservation of the energy of the exhaust gas. Below, we shall use the subscripts *in* for the flow parallel to the inlet channel, *out* for the flow parallel to the outlet channel and *w* for flow through the soot layer and the wall.

The exhaust gas mass balances state that, at each axial point of the inlet channel, the change of the exhaust gas flow is equal to the flow leaving the inlet channel via the porous wall. An exactly analogous balance is defined for the outlet channel.

$$\frac{\partial}{\partial z}\left(\rho_{in}u_{in}\right) = -\left(4/\ell\right)\rho_w u_w, \qquad \frac{\partial}{\partial z}\left(\rho_{out}u_{out}\right) = +\left(4/\ell\right)\rho_w u_w \tag{20}$$

The balance equation for the axial component of the momentum of the gas states that the axial pressure variation is due to convective transport of the z-component of momentum and the viscous drag forces exerted in the gas flow. The balance equation is the same for both channels.

$$\frac{\partial p}{\partial z} + \frac{\partial}{\partial z}\left(\rho_i u_i^2\right) = -\frac{a\mu u_i}{d_h^2}, \qquad i = in,\ out \tag{21}$$

where d_h is the hydraulic diameter of the channel, which, for square channels, is equal to the channel's edge: $d_h = \ell$. The viscous drag is caused because there is a gradient of the axial velocity of the gas, as axial velocity reduces to zero at the walls. According to Bissett [6], these drag forces should be near those observed for an impermeable wall, because only a small fraction of the gas penetrates the wall at each axial point.

The above balances, together with the Darcy correlation (19), are used to calculate the distribution of the gas velocities in the inlet and outlet channels and the velocities normal to the soot layer and wall.

Once the velocities distribution has been calculated, the model computes the energy exchanged between the gaseous and solid phase porous wall. The energy balances for the inlet and outlet channels are:

$$c_{p,g}\frac{\partial}{\partial z}\left(\rho_{in}u_{in}T_{in}\right)=-\left(4/\ell\right)c_{p,g}\rho_w u_w T_{in}+h_{in}\left(4/\ell\right)\left(T-T_{in}\right)$$
$$c_{p,g}\frac{\partial}{\partial z}\left(\rho_{out}u_{out}T_{out}\right)=-\left(4/\ell\right)c_{p,g}\rho_w u_w T_w+h_{out}\left(4/\ell\right)\left(T-T_{out}\right) \quad (22)$$

The balance for the outlet channel differs in the second term that concerns energy transport via the flow through the porous wall. Apart from the sign of the term, the temperature is different, because the gas leaving the porous wall has the temperature of the wall.

Finally, the axial temperature distribution along the wall is calculated. The heat balance implements 1D heat conduction and source terms are because of gas–solid heat convection and reaction exothermy.

$$\left(\rho_p c_{p,p}+\rho_s c_{p,s}\right)\frac{\partial T}{\partial t}=\lambda\frac{\partial^2 T}{\partial z^2}+h_{in}\left(4/\ell\right)\left(T-T_{in}\right)+h_{out}\left(4/\ell\right)\left(T-T_{out}\right)+\frac{1}{V_p+V_s}\frac{dQ}{dt} \quad (23)$$

In the above equation, the heat source term *dQ/dt* expresses heat exchange due to perpendicular gas flow and reaction exothermy; it is given by eq. (16). Since this term refers to an axial element of length Δz, as seen in Figure 3, it is devided by the sum of the elementary volumes of the substrate and the soot layer V_p+V_s, defined in equations (3a) and (3b) respectively.

2.7 3-D modeling of heat conduction and inlet flow distribution

One-dimensional channel models assume that all channels of the filter operate under identical conditions. The three-dimensional modeling raises this assumption by accounting for three main phenomena that are neglected by 1-D modeling, namely, heat conduction between channels, heat losses to the ambient air, and non-uniformity of mass flow rate at the channels inlet. Also, it takes into account the non-symmetric structure of the specific filter, which is made up of smaller SiC filter blocks, arranged in a Cartesian grid and glued together using a special adhesive cement layer (Figure 4). The cement layer has different thermophysical properties than the SiC (see Table 2).

For the calculation of the 3D temperature field in the filter, the heat diffusion equation in three dimensions should be solved, which is [22]:

$$\rho_s c_{p,s}\frac{\partial T}{\partial t}=\nabla\cdot\left(\lambda\nabla T\right)+\dot{q}_{total} \quad (24)$$

The source term $\dot{q}_{total}$ is the sum of all heat sources in the model. It is given by the sum of heat exchanged due to chemical reactions and convection owing to the flow *through* the soot layer and the wall [dQ/dt of eq. (16)], and the heat convected between the solid phase and the gas flow in the inlet and outlet channels that is *parallel* to the wall.

$$\dot{q}_{total}=h_{in}\left(4/\ell\right)\left(T-T_{in}\right)+h_{out}\left(4/\ell\right)\left(T-T_{out}\right)+\frac{1}{V_p+V_s}\frac{dQ}{dt} \quad (25)$$

The solution of the three-dimensional heat balance (24) is accomplished by the finite element code, which calculates the three-dimensional temperature field in the filter relying on the 1-D model to provide the heat source terms involved in the balance. This requires the interfacing of the FEM code with the 1-D core model. The interfacing is possible using the User Programmable Feature (UPF) functionality of the FEM software suite that allows the user to write custom functions for properties or source terms of the elements. Such user subroutines are customarily written in FORTRAN, which is also the language of the CATWALL code implementation [11]. The calculation of the non-uniform temperature field in the filter allows the model to account for the so-called partial regenerations, that may leave significant portions of the deposited soot unburned, because of unfavorable conditions for regeneration propagation. Partial regenerations affect the distribution of the flow field at the inlet of the filter, since the flow is then channeled through the low flow resistance areas of the filter. A submodel has been included to take into account this effect. According to this submodel, the filter channels are viewed as a set of flow resistances in parallel. The objective of the submodel is to distribute the total mass flow rate at the inlet of the filter so that the pressure drop induced from each channel is the same. In fact, not every channel of the filter is treated separately, because of the excessive computational power required. Rather, the model separates sectors of channels that are treated identically. These sectors correspond to the meshing of the filter that is used from the FEM code for the temperature field calculation.

For the determination of the pressure drop of each channel sector, eqs. (19) and (21) are used. Because of the quadratic term of eq. (21) and the dependence of physical properties on the pressure and temperature of the gas at each point, the pressure drop Δp_i for each sector of channels is a non-linear function of the mass flow rate $\dot{m}_i$ at the inlet of the sector: $\Delta p_i = f(\dot{m}_i)$. Moreover, there is not a closed expression for the function *f*, and, given $\dot{m}_i$, the pressure drop Δp_i may only be calculated by a trial-and-error procedure, following the usual procedure for pipe networks [23]. Nevertheless, the function *f* is *nearly* linear, because the pressure losses are mainly induced by the gas flow through the soot layer and the wall (eq. 19). Therefore, the total pressure losses for each channel may be approximately computed by a relation of the form $\Delta p_i = R_i \dot{m}_i$, where R_i is the flow resistance of the sector.

This fact has been exploited in order to develop an iterative procedure to compute the flow distribution at the filter inlet. The procedure features the following steps [24]:

Step 1. Provide an initial guess for the flow rate $\dot{m}_i$ of each sector. Assuming that the cross-sectional (frontal) area of each sector is A_i, we assume that $\dot{m}_i = \dot{m}\frac{A_i}{A}$ (uniform flow distribution).

Step 2. Calculate the induced pressure drop for each sector $\Delta p_i = f(\dot{m}_i)$.

Step 3. Calculate the approximate linear resistance R_i for each sector: $R_i = \Delta p_i / \dot{m}_i$.

Step 4. Calculate the approximate linear resistance of the whole filter: $\frac{1}{\overline{R}} = \sum_{i=1}^{N} \frac{1}{R_i}$

Step 5. Calculate an approximate value for the pressure drop of the whole filter: $\Delta p = \overline{R}\dot{m}$.

Step 6. Calculate new values for the flow rates of each sector: $\dot{m}_i' = \frac{\Delta p}{R_i}$

Steps 2–6 are repeated until a set of flow rates for each sector is obtained so that the calculated induced pressure drop $\Delta p_i = f(\dot{m}_i)$ for every sector is the same. The above iterative procedure converges quickly (usually after 3 to 10 iterations) to the desired set of mass flow rates.

3 3-D heat transfer calculation

The approach selected to solve the problem of the calculation of the 3-D temperature field of the filter was to interface CATWALL with the commercial FEM software, by developing (a) a model of the diesel particulate filter in the ANSYS environment and (b) a set of interface subroutines that handle the task of data interchange between the two codes [24,25].

3.1 ANSYS solid and finite element model of the filter

The solid model is the description of the geometric shape of the filter. The volumes comprising the solid model are then assigned material properties. The solid model is then meshed to generate the finite element model that is actually used by the FEM solver. The front of the solid model of the filter is given is Figure 4. Usually, a quarter of the cylindrical filter needs to be modeled only, because of the symmetry of its structure. The solid model comprises different volumes for the main part of the SiC filter blocks, the inlet and outlet regions of the blocks (where the plugs are), the adhesive of the filter blocks, the insulation mat and the canning. Depending on the volume, different material properties are assigned (that is, heat capacity, thermal conductivity and density).

Evidently, for simplicity and speed of the computation, the solid model of the filter is simplified, in the sense that the details of the filter structure, with its grid of channels and plugs, is replaced by continuous volumes. This approach necessitates the use of bulk quantities for the density and the heat conductivity of the SiC filter blocks, which are computed using the void fraction of the filter structure:

$$\rho_{bulk} = \varepsilon \rho_{SiC} \qquad \lambda_{bulk} = \varepsilon \lambda_{SiC} \tag{26}$$

Because of the presence of the plugs, the void fraction ε_{plug} of the inlet and outlet regions of the filter blocks is different from the void fraction of their main part. Therefore, separate volumes are defined for the plug regions of the solid model. These volumes are assigned the bulk density and heat conductivity of the plug regions that were computed using ε_{plug} instead of ε. The (real and bulk) temperature dependent material properties of the SiC, adhesive, insulation mat and canning that were used in this work are given in Table 2. In the second view of Figure 4, one brick of the SiC filter as

well as its surrounding adhesive have been removed, to reveal the different volumes of the solid model that correspond to the main and the plug region of the filter.

ANSYS meshes the solid model to construct the finite element model of the filter, which consists of elements and nodes. The element type that was chosen for meshing was SOLID70, which is a thermal solid element with eight nodes, with a single degree of freedom, temperature, at each node. The meshed finite element model of the specific filter that has been used in this work is illustrated in Figure 5. In conjunction with grid generation, two fundamental points have to be noted: First, there is no restriction—that is imposed from the 1-D regeneration model—regarding the cross-sectional shape of the elements. Each row of elements along the axial direction that corresponds to SiC (see Figure 5) is referred to as a sector. The obvious implication is that the 1-D code should be invoked as many times as the number of sectors, namely the number of elements at a cross-section of the filter. Thus, the finer the grid, the more times the 1-D model will be invoked, with direct consequences to the computational cost of the model. Second, the grid designed for the FEM analysis must be orthogonal along the axial direction, with fixed element length, which is an integer multiple or submultiple of the discretization length Δz of the 1-D code. Essentially, the finite element model of the face is extruded along the axial direction in order to produce the total finite element model. The requirement for axial orthogonality is imposed by the structure of the filter itself, while the fixed element length is imposed by a limitation of the 1-D code, which operates on a fixed axial discretization interval Δz. The above two requirements must be met, so that a mapping of the 1-D code and the ANSYS grids is possible, so that heat source and temperature information may be exchanged between the two grids. The latter point brings into the foreground the issue of interface implementation, which is discussed below.

3.2 Interface implementation

Through the interface between the two codes, the element number, temperature, heat source terms and time are communicated. Essentially, the FEM software gives the current time, element number and element temperature as input to the main interface subroutine, and expects to receive the element heat source term. The heat source terms are employed by the FEM software in order to compute the new temperature field in the filter. The task for the interface subroutines is to convert ANSYS input so that it is sensible for the 1-D code, subsequently call the 1-D code for the calculations, and finally re-convert 1-D code output and feed it back to the FEM software.

The concept of the interfacing is given schematically in Figure 6. It is evident that the implementation of two basic modules was required, because of the non-compatible operation and grid design of the two codes. The restrictions of the grid design and the functionality of the two basic modules is discussed in brief below.

Grid mapping module. There are two co-existing (though incompatible) grids for the filter: The FEM grid consists of elements (and nodes for each element) while the 1-D code grid consists of sectors and nodes for each sector. Therefore, a mapping procedure must be implemented between the two grids to achieve exchange of information. Specifically, the procedure uses the internal numbering

of elements of the FEM software. If the length for axial discretization is the same for both the FEM grid and the 1-D code grid, then each element number also corresponds to a single pair of CATWALL sector and node numbers. In this case, there is a one-to-one correspondence between the two grids, which also applies to the heat source and temperature data.

If the 1-D code grid is finer than the FEM grid (the usual case) then one element number corresponds to a set of 1-D code nodes. In this case, the sum of heat sources from the 1-D code is given to the FEM code as the element heat source term, and temperature data passed to the 1-D code is assumed equal for all nodes corresponding to the specific element. The situation is inversed if the 1-D code grid is coarser than the FEM grid. Then the heat source calculated for a single 1-D code node is divided to the corresponding the FEM code elements, and the 1-D code node temperature is computed as the average of the corresponding element temperatures. These considerations should make clear why the discretization length of the FEM grid along the axial direction must be an integer (sub) multiple of the 1-D code discretization length.

Field buffering module. The FEM software may call the user subroutine more than once for each element. Each time that the user subroutine is called, the heat source term is requested and temperature is supplied back as a result for the next time step. Nevertheless, it is not efficient in terms of computational power to call the 1-D code for the sector to which the element belongs each time the FEM software requires it. The reason is that the 1-D code operates on the whole sector and not on a per-node basis. Therefore, a special module was implemented, which buffers the temperature and heat source fields. Whenever the FEM software takes a new time step, the 1-D code is called as many times as the numbers of the sectors, and the resulting heat source field is stored in a buffer. Subsequently, when a heat source term is requested, it is extracted from the buffer and passed to the FEM software. The temperature value that returns from the FEM software is stored to the temperature field buffer. At the next time step of the FEM software, the temperature field is passed from the buffer to the 1-D code and the next heat source field is computed.

3.3 Solution procedure

The heat losses of the filter to the surrounding air are taken into account by imposing surface convective boundary conditions on the external nodes of the filter model. The value of the heat transfer coefficient between the filter's canning to the ambient air depends on the specific filter layout in exhaust system and vehicle speed, usually being in the range 20–100 W/(m^2K). The highest values of the range typically include the effect of radiation exchange to the surroundings which becomes important when the can surface temperature exceeds 400^{o}C.

An indicative running time of 2 seconds per 1 second of real filter operation is observed for meshing used in this work, which features 144 × 50 = 7200 elements in total (144 elements on each cross-section) for the whole filter, which includes the 5.66" × 6" SiC/ adhesive filter structure, the insulation mat and the canning.

Finally, a significant advantage of interfacing the 1-D filter regeneration code with FEM software to calculate the three-dimensional temperature field is the ability to carry out thermomechanical analysis. Calculation of thermal stresses in the filter is a very important feature of the model, since crack formation due to thermal stresses is a common reason of filter failure. Details of the stress analysis procedure are presented in [4]. Similar to the thermal analysis, the cell structure of the filter is modeled by a "homogenized" isotropic linear elastic material with Young's modulus E=19 GPa, Poisson's ratio v=0.15, thermal expansion coefficient α=4·10^{-6}/°C and mass density ρ=0.72 gr/cm^3. The adhesive is modeled also by an isotropic linear elastic material with E=1.5 GPa, v=0.2, α=2.7·10^{-6}/°C and ρ=1.26 gr/cm^3

4 Exploitation of the 3-D model results in detailed filter design

The assessment of the model's capabilities was based on the results of engine bench loading–regeneration experiments performed on one of the Laboratory engine test benches. The filter employed in these experiments was a 200 cpsi SiC filter fitted in the exhaust pipe of a 2-liter displacement HDI turbocharged passenger car engine, about 600mm after turbine exit. Engine and Diesel filter specifications are summarized in Table 3. Exhaust temperatures were measured simultaneously, at the inlet and the exit of the filter, and inside the filter, along a filter diameter 15 mm deep from filter exit. Thermocouples are placed in the center of each filter block, along the diagonal of the filter. The exhaust emissions of CO, CO_2, NO_x and HC were measured simultaneously before and after the filter. The O_2 concentration was calculated by the A/F ratio obtained from the UEGO sensor installed before the filter inlet. The experimental layout of the filter loading–regeneration experiments is presented in Figure 7.

The kinetic parameters of the rate expressions that were used in this work were obtained by a validation study of the 1-D model [10]. In its turn, the latter study was supported by an extensive set of TGA analysis experiments of soot samples taken directly from the filter [26]. Values of the pre-exponential factor and the activation energy of each reaction are given in Table 4. In brief, the values of activation energies for catalytic oxidation correspond to dry soot oxidation for samples where the VOF content varies in the range between 2.5 and 8%. The pre-exponential factors were obtained by allowing a certain amount of tuning. Furthermore, the wall permeability, soot density and soot permeability times density that were inserted in the 1D model to simulate the pressure drop behaviour of the validation experiments had the following values: Wall permeability $K = 2 \cdot 10^{-13}\ \mathrm{m}^2$; Soot density $\rho_p = 80\ \mathrm{kg/m}^3$; and soot permeability times density $\left(\rho K_p\right) = 2.2 \cdot 10^{-11}\ \mathrm{kg/m}$.

In order to demonstrate the role of the 3-D filter regeneration model in the process of detailed filter design, a simulation of the case of Figure 8 has been carried out. Obviously, compared to the limited information that may be obtained by the four thermocouples of the experiment, the code yields an excessive amount of information. Three-dimensional temperature fields, temperature-gradient fields for any direction and inlet flow profiles are exited by the code and may be viewed for any filter section.

As a first step, eight snapshots of temperature fields for a section of the filter are presented in Figure 9. The elements of the canning, the insulation mat, the surrounding adhesive and one SiC block of the filter have been removed, to comparatively view regeneration characteristics in the center and the periphery of the filter. The onset of regeneration is observed near the filter exit, where the maximum temperatures are also observed. It becomes apparent that the evolution of regeneration in each one of the small periphery blocks is significantly different from that of a central block. Regeneration in the periphery of the filter is delayed, presumably due to the increased heat losses to the ambient air combined with the insulating effect of the adhesive surrounding the filter block, which inhibits the radial propagation of heat released in the central blocks. Thus, the specific design with periphery blocks is a bad design resulting in sustained incomplete regeneration.

Nevertheless, as illustrated in Figure 8, the computed delay in the regeneration of the outlet blocks of the filter is significantly less than that measured delay of about 5 minutes. It is beyond the capacity of the model in its current state to accurately predict this delay. Possible causes for the discreapncy could be the following: First, the regeneration model lacks a mechanism to include the effect of the soot's VOF, which may be responsible for this type of regeneration, because it seems insensitive to the regeneration occurring in the inner filter block and seems more connected to the gradual elevation of the inlet gas temperature. Second, the initial filter temperature distribution and accumulated soot distribution may be significantly inhomogeneous, while the model assumes that the above distributions are uniform. Third, uncertainties regarding the thermophysical properties of the filter materials and especially the soot layer may negatively influence the model's predictive ability.

A second step in the detailed study of the filter regeneration behaviour is the study of temperature gradients. In Figure 10, the magnitude of the thermal gradient is plotted for three characteristic time points. The maximum temperature gradients of the inner filter block are initially observed near the outlet of the filter, at the boundary where the channels' plugs start. This is a consequence of the higher heat capacity of the filter in the plug region. As the regeneration moves to the periphery of the filter, the same happens with the thermal gradients. Maximum thermal gradients are predicted at the small periphery block at the interior cement–SiC interface. Later on, thermal gradients gradually diminish, although their maximum values still remain at the small periphery block of the filter.

The temperature gradient fields are employed in the computation of the thermal stress field of the filter. This process has discussed in more detail in [4]. Maximum thermal stresses of the order of 20 MPa have been computed in severe filter failure scenarios like that of Figure 1. Such levels of thermal stresses lead to the failure of the filter material by cracking, as confirmed by the full-scale experiments. Thus, the identification of high thermal stress concentrations areas like those of Figure 10 is very important for improvements in the detailed design of the filter.

The third step taken in this study is the examination of the flow profiles at the inlet of the filter, as affected by filter loading maldistribution. Specifically, incomplete regenerations lead to prominent flow maldistribution, which depends on the non-uniformity of the soot layer distribution and the

corresponding flow resistances. To quantify this effect, we define an index of the mass flow rate non-uniformity for each brick, as follows:

$$\gamma = \frac{\text{flow entering the brick}}{\text{flow that would enter the brick if the flow profile were uniform}} = \frac{\dot{m}_i}{\dot{m}\frac{A_i}{A}}$$

The above index is unity for uniform flow. Values greater than unity imply higher mass flow rates than those expected with from a uniform inlet flow profile, and vice-versa.

In Figure 11, this index is plotted through the first 500 s of the simulation for the four bricks that comprise the quarter of the filter. In the beginning of the simulation, all channels are assumed uniformly loaded with particulate, therefore the non-uniformity index equals unity for all bricks. However, during the regeneration, the model predicts a significant non-uniformity of the flow. Specifically, the flow is channeled mainly through the central brick of the filter, since regeneration occurs there first. Mass flow rates through the center brick are approximately double compared to those at the filter periphery. The above results of the inlet flow distribution are aligned with the experimental findings presented in [12,17].

A more detailed view of the non-uniformity of the inlet flow is also given in Figure 12, where two snapshots of the percentage of the flow entering each sector of the model is presented. It is noticeable that the model also predicts a mass flow rate profile across each filter block, which declines towards the outlet of the filter. This effect is the result of the temperature field within the filter. Temperatures decline at the filter periphery due to the losses to ambient air, and thus less soot mass is consumed and the flow resistance is higher. The flow non-uniformity becomes milder after regeneration propagates to the periphery of the filter. It is important to note, though, that, according to Figure 11, the flow profile remains non-uniform after the end of the regeneration. This may be due to incomplete regeneration in the periphery, but also to residual temperature differences remaining in the monolith that cause differences in exhaust gas density and thus mass flowrate among the channels. This flow maldistribution has an impact to the total pressure drop induced by the filter, and is connected to the problem of estimating the soot load level of the filter employing pressure drop measurements. As a further example, an attempt is made to compute the evolution of the medium flowrate regeneration of Figure 13. In this case the 3-D model successfully predicts the evolution of regeneration and the phase shift between center and periphery, (Figure 14) with the same kinetics parameters already presented in Table 4. The 1-D model predictions are also inserted in Figure 14 for comparison.

Of course, the development of a 3-D regeneration model is not intended to substitute the 1-D model, since the scope of each model is different. Rather, the two models should be viewed as complementary tools. As mentioned above, the application of the 3-D model is based on the original tuning of the reaction kinetics performed by the 1-D model, to save computation and manpower cost. Furthermore, the 1-D model is useful in the initial stage of the exhaust system design, where it should provide a rough view of the overall performance characteristics of the filter. The need for 3-D modeling comes to the foreground in detailed filter design and optimization studies, when local

phenomena and especially thermal stress calculations are of interest. In its current state of development, and despite the acknowledged limitations, the 3-D filter regeneration model provides insight to the evolution of regeneration in the modular SiC filter and may be used for the determination of stress concentrations and the effect of critical material properties. This could be a valuable aid towards the identification of design flaws and decisive directions for research.

5 Conclusions and Future Work

A 3-D modeling approach for the catalytic regeneration of diesel filters was developed by interfacing a one-dimensional catalytic regeneration filter channel model with commercial FEM software. The 1D base features a reaction scheme for thermal and catalytic regeneration. It has already been tested and validated extensively against characteristic cases, including failure scenarios.

The 3-D model is enhanced with a module for the determination of the flow distribution among the different channels of the filter. It extends the potential of the model towards the prediction of the full temperature field within the filter, the non-uniformity of the flow and the effect of incomplete filter regeneration to the pressure drop of the filter. Also, stress analysis and determination of stress concentrations in the detailed design of diesel filters of modular design, with highly anisotropic structure can be carried out based on the above. Characteristic validation cases are presented in this paper, to demonstrate its capabilities and weak points. The limitations of the model are illustrated by purposely selecting a difficult test scenario to demonstrate the effects of the Volatile Organic Fraction content of the soot at low flowrates.

It should become clear by the overall presentation that the development and validation of workable engineering models for Diesel filter regeneration is significantly more demanding than the development of their computational cores that are usually published in the literature with simple validation test cases. Nevertheless, engineering models are already essential in engineering design of Diesel filter systems and their accuracy and application range is constantly improving to address challenging design optimization tasks.

Acknowledgements

The authors would like to thank their collaborators, George Stratakis and George Konstantas, for supplying experimental data and running a number of simulation cases, as well as Sungtae Hong of IBIDEN Co. Ltd. for his useful discussions and comments, and assistance with ANSYS simulations.

List of Symbols

A	1. Pre-exponential factor of reaction rate expression, [mol/m^{3}s]
	2. Cross-sectional area of the soot layer , [m^2]
c_p	Specific heat capacity, [J/kg·K]
d_h	Hydraulic diameter of channel, [m]
E	Activation energy of reaction rate expression, [J]
ΔH	Molar heat of reaction, [J/mol]
h	Heat transfer coefficient, [W/m^{2}K]

k	Arrhenius-type rate factor, [mol/m^{3}s]
ℓ	Length of inner channel edge, [m]
$\dot{m}$	Exhaust gas mass flow rate, [kg/s]
M	Molecular mass, [kg/mol]
p	pressure [Pa]
q	Heat flux, [W/m^3]
Q	Heat , [J]
r	Rate of reaction, [mol/m^{3}s]
R_g	Universal gas constant, [8.314 J/mol·K]
t	Time, [s]
T	Temperature, [K]
u_z	Exhaust gas velocity, [m/s]
V	Volume, [m^3]
w	Thickness, [m]
y	Oxygen molar fraction, [–]
z	Distance from the filter inlet, [m]

Greek Letters

ε	Void fraction
λ	Thermal conductivity, [W/m·K]
μ	Viscosity
ρ	density, [kg/m^3]
ψ	fractional extent of the catalytic additive oxidation, [–]
ξ	total concentration of catalytic additive in the soot layer, [mol/m^3]

Subscripts

g	gas
in	inlet channel
out	outlet channel
p	particle (soot) layer
s	substrate
w	wall

Abbreviations

DI	Direct Injection
DPF	Diesel Particulate Filter
EGR	Exhaust Gas Recirculation
HC	Hydrocarbons
HDI	High pressure Direct Injection
LTTE	Laboratory of Thermodynamics and Thermal Engines
mfr	Exhaust gas Mass flow rate
TF	Temperature of filter
T/C	Thermocouple fitted on experimental layout
TGA	Thermo-Gravimetric Analysis
VOF	Volatile Organic Fraction

Table 1 Reactions and rate expressions of the regeneration model

	Reaction	Rate expression
1	$C + O_2 \longrightarrow CO_2$	$r_1 = k_1 y$
2	$C + 0.5O_2 \longrightarrow CO$	$r_2 = k_2 y$
3	$C + 4CeO_2 \longrightarrow 2Ce_2O_3 + CO_2$	$r_3 = k_3 \psi$
4	$C + 2CeO_2 \longrightarrow Ce_2O_3 + CO$	$r_4 = k_4 \psi$
5	$Ce_2O_3 + 0.5O_2 \longrightarrow 2CeO_2$	$r_5 = k_5 (1 - \psi) y$
	where: $k_i = A_i e^{-E/R_g T}$, $i = 1 \ldots 5$	

Table 2 **Thermophysical properties of SiC, adhesive, insulation mat and canning**

	SiC				adhesive		insulation		canning	
Temperature [°C]	real	λ bulk (main)	bulk (plug)	c_p	λ	c_p	λ	c_p	λ	c_p
25	57.1	21.4	39.3	686	0.187	740	0.04	1190	15.2	466.5
250	35.4	13.3	24.4	1005	0.222	1012	0.05	1190	19.4	538.2
500	24.6	9.2	16.9	1123	0.241	1141	0.08	1190	22.4	588.1
7500	19.8	7.4	13.6	1182	0.242	1188	0.12	1190	24.5	623.8
1000	15.0	5.6	10.3	1219	0.302	1200	0.17	1190	26.2	651.7
1250	13.0	4.9	8.9	1230	0.350	1205	0.23	1190	27.5	670.0
		ρ			ρ		ρ		ρ	
	1800	675	1238		137		300		7900	

Units: λ [$Wm^{-1}K^{-1}$], c_p [$J\,kg^{-1}K^{-1}$], ρ [$kg\,m^{-3}$].

Void fractions for the calculation of bulk values: $\varepsilon = 0.375$, $\varepsilon_{plug} = 0.688$

Table 3. Engine technical data and diesel filter specifications

Engine type	HDI turbocharged engine
Cylinders	4, in-line
Displacement	1997 cm^3
Rated power /rpm	80 kW/4000 rpm
Rated torque/rpm	250 Nm/2000 rpm
Filter Type	SiC 14/200 cpsi (cells per square inch)
Filter Diameter x length	143.8 mm x 150 mm
Cell pitch	1.89 mm
Filter Wall thickness	0.4mm

Table 4 Kinetic parameters of the model's reaction rates

	Reaction	Pre-exponential factor (A) ($mole/m^3$,s)	Activation Energy (E) (kJ/mole)
1	$C + O_2 \longrightarrow CO_2$	1E13	190
2	$C + 0.5O_2 \longrightarrow CO$	5.5E10	150
3	$C + 4CeO_2 \longrightarrow 2Ce_2O_3 + CO_2$	4.5E11	120
4	$C + 2CeO_2 \longrightarrow Ce_2O_3 + CO$	4E8	80
5	$Ce_2O_3 + 0.5O_2 \longrightarrow 2CeO_2$	1E12	80

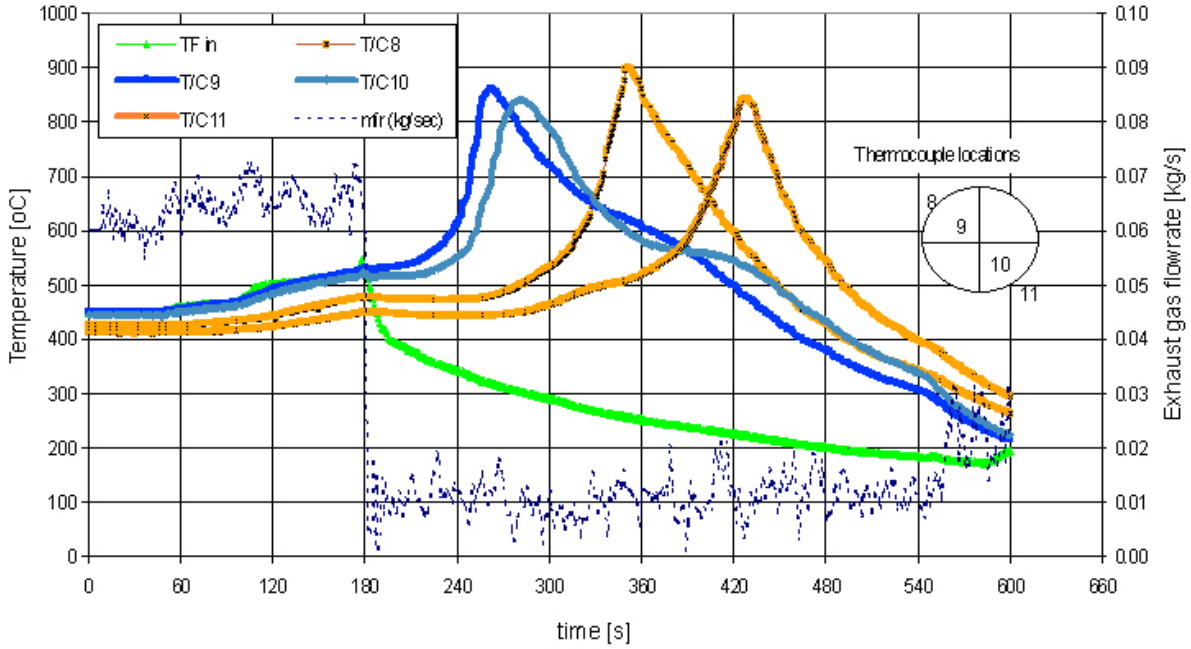

Figure 1. Deceleration test with fuel additive. Initial SiC filter soot loading: (est.) 29g. Initial engine operation at 2500 rpm–engine load 80 Nm, filter inlet temperature 500°C. Step decrease at t=180s to 800 rpm–load 20 Nm.

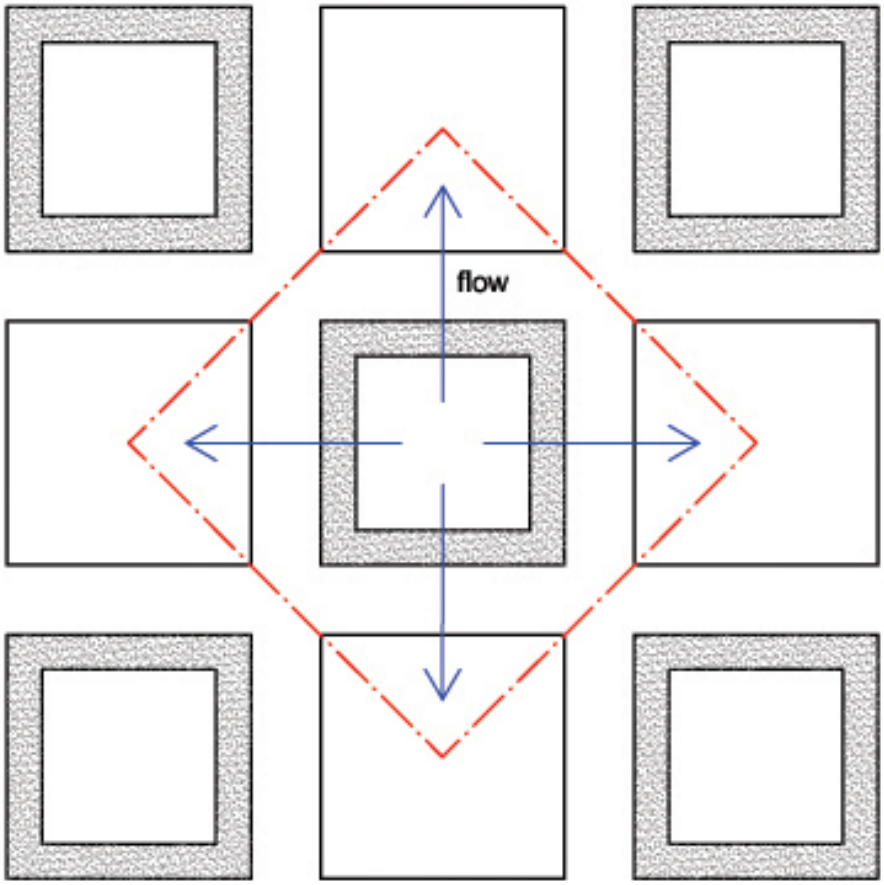

Figure 2. **Computational cell for a wall flow diesel particulate filter, consisting of one inlet channel and four adjacent outlet channels.**

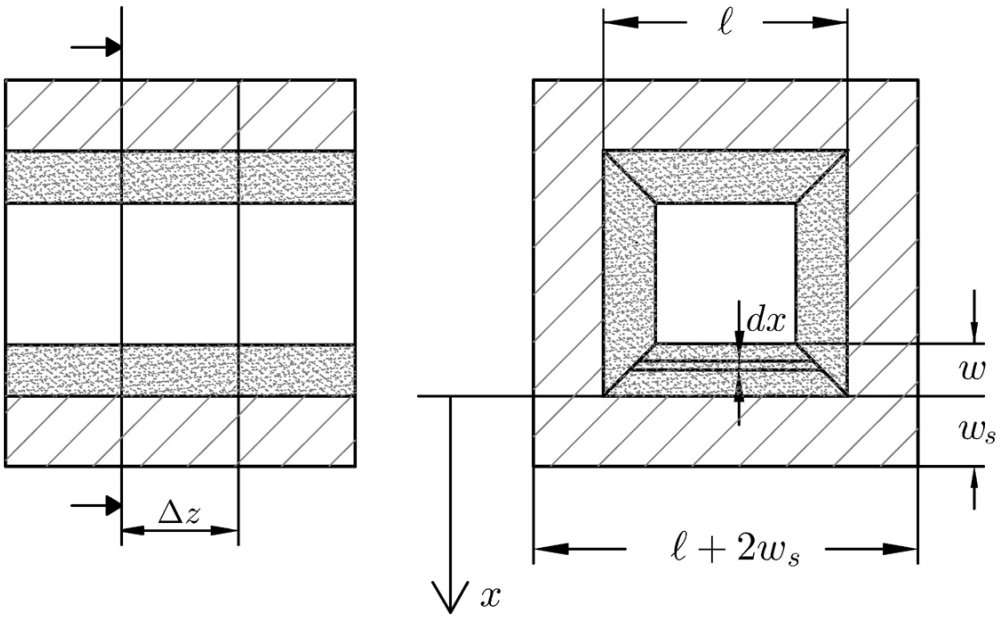

Figure 3. Schematic representation of the cross section of a loaded wall flow channel assuming that the soot layer consists of four trapezoids.

(a)

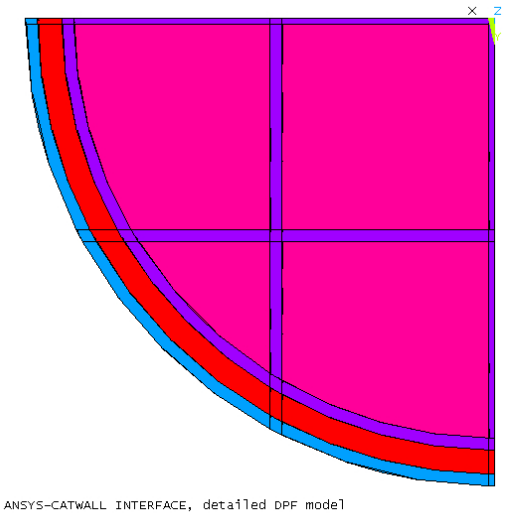

(b)

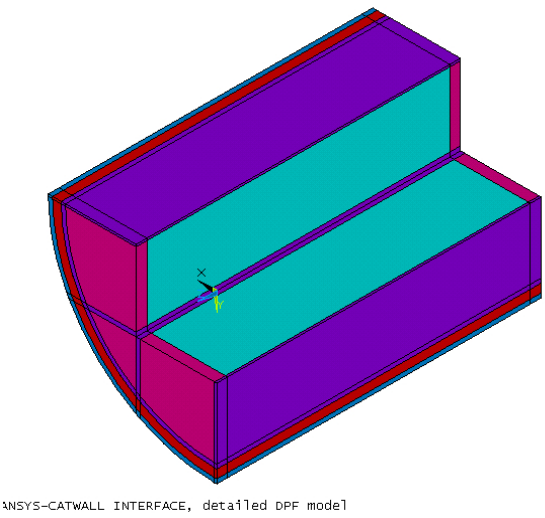

Figure 4. Solid model of the filter. Different materials are designated by different colors.
(a) Front view: blue=canning, red=insulation, purple=adhesive, magenta=SiC – plugs' region
(b) Side view, with the central filter block and adhesive removed. The different materials for the plug region (magenta) and the main region (cyan) of the SiC filter blocks are visible.

(a) (b)

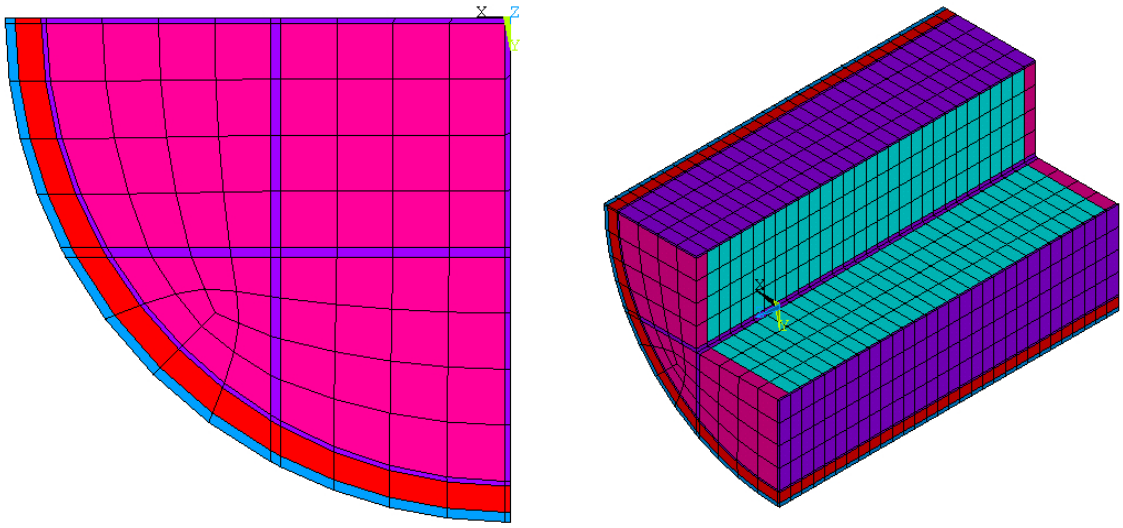

Figure 5. Finite element model of the filter, produced after meshing the solid model.
(a) Front view.
(b) Side view, with the central filter block and adhesive removed.

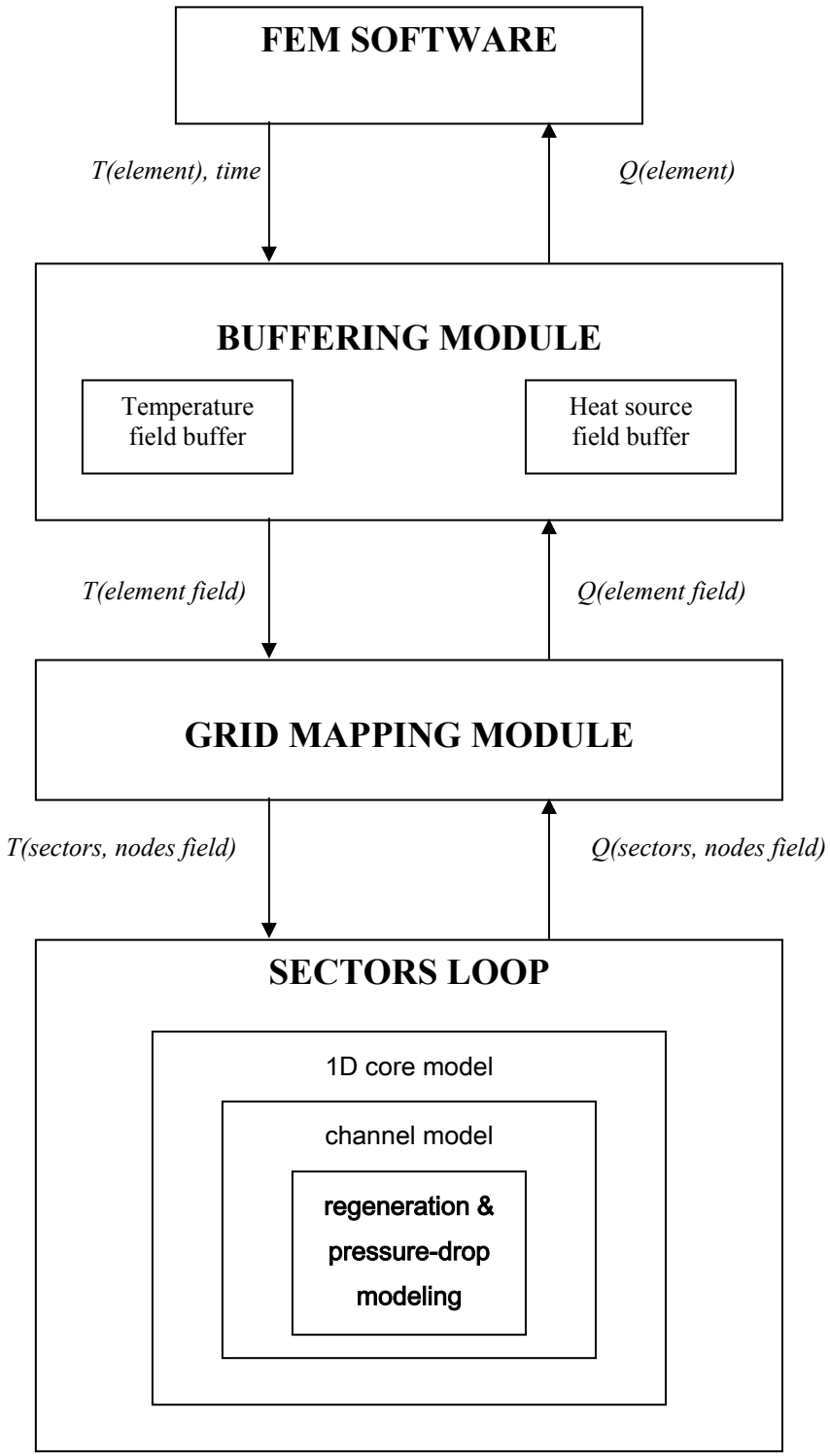

Figure 6. ANSYS–CATWALL interfacing concept (flow diagram)

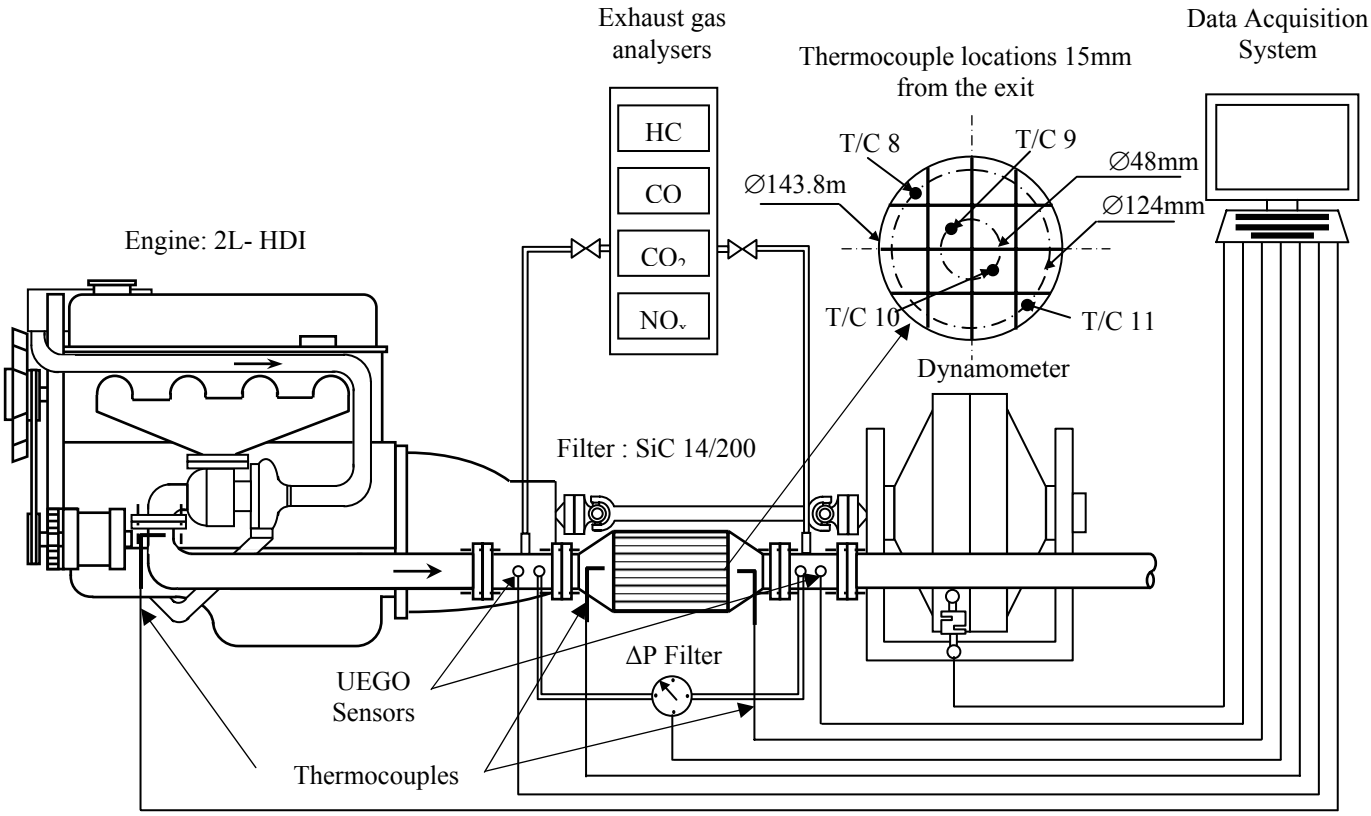

Figure 7. Experimental layout. Engine and digitally controlled dynamometer installation is shown along with exhaust gas analysers, main filter measurement lines, and data acquisition system.

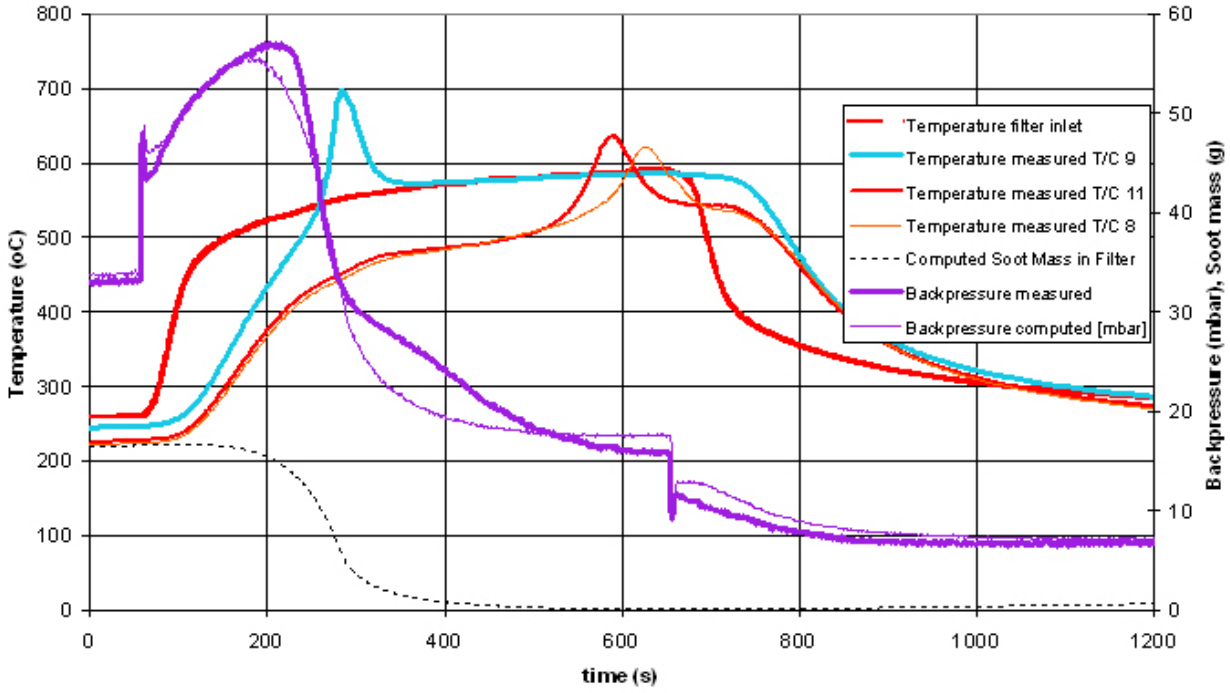

Figure 8. **Low mass flow rate regeneration case: Evolution of exhaust temperature at filter inlet, filter exit wall temperature at three characteristic points (Thermocouples 8,9,11, see Figure 7), computed evolution of soot mass in the filter, measured and calculated filter backpressure.**

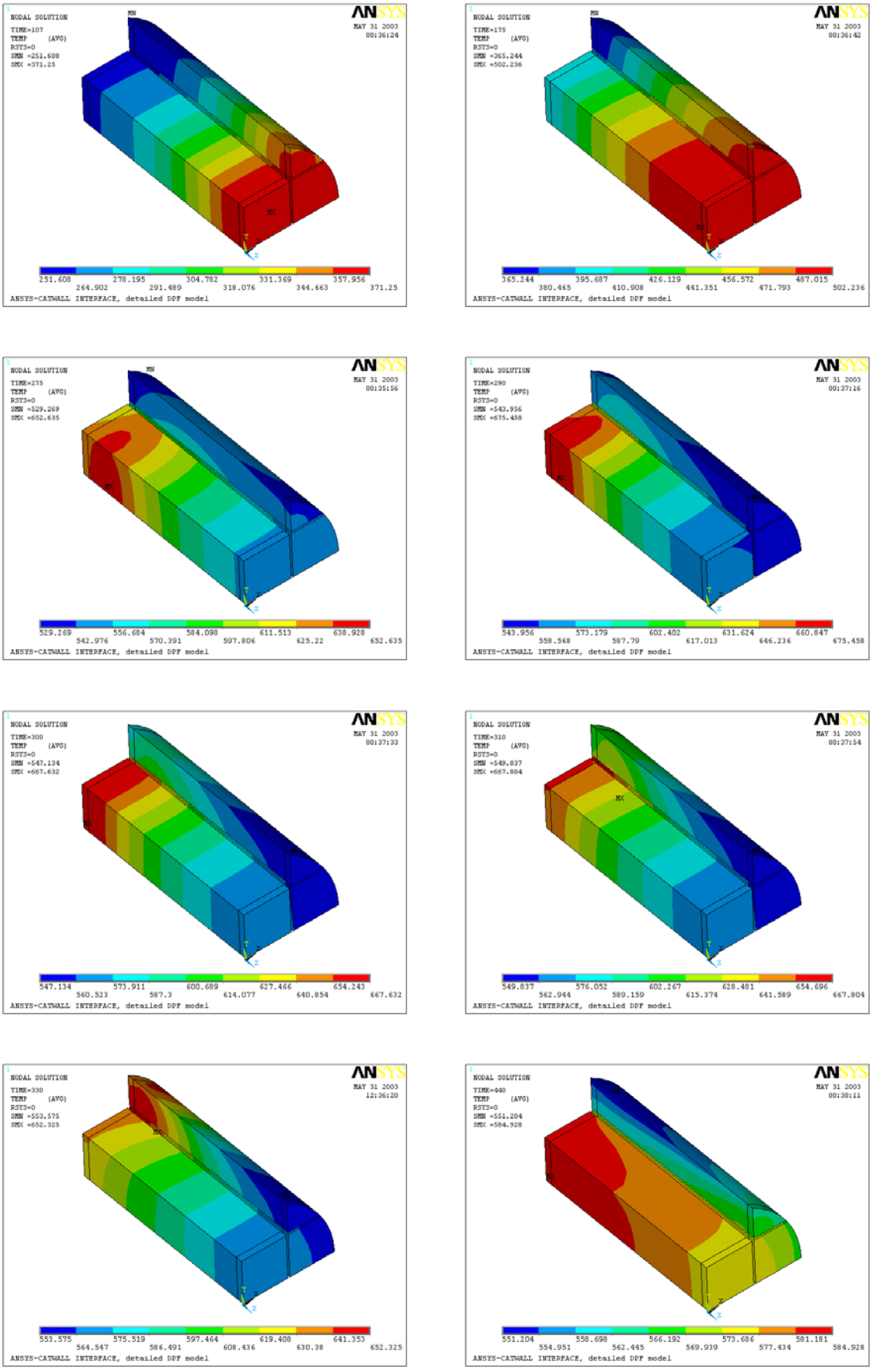

Figure 9. Sequence of snapshot views of the predicted 3D temperature field of the SiC, in the interior of the filter, at the SiC – adhesive cement boundary (for the regeneration experiment of Fig.8)

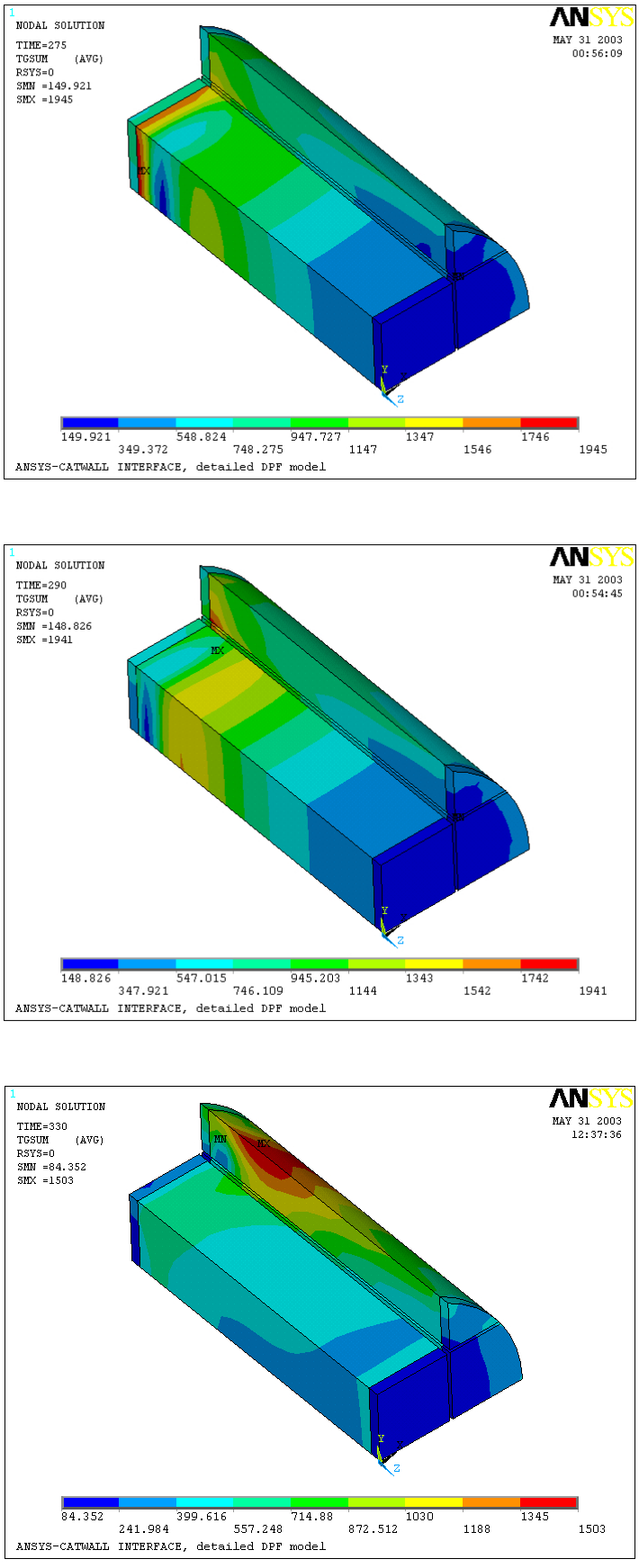

Figure 10. Computed 3D temperature gradient field in three characteristic time points (t= 275, 290 and 330 s) for the regeneration test case of Figure 8

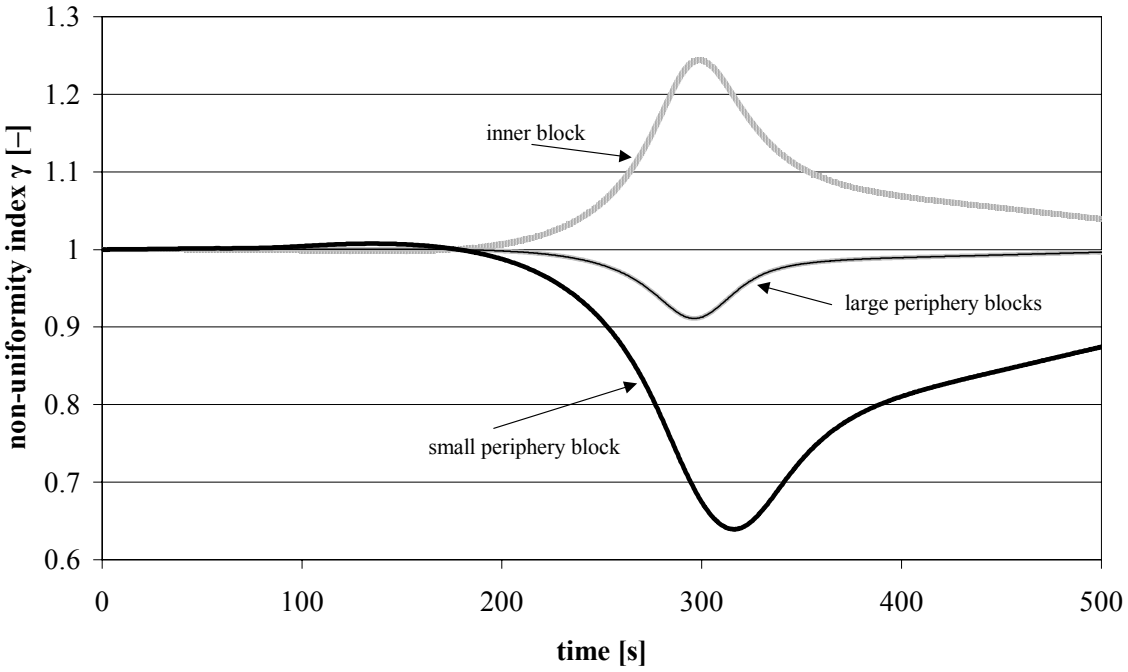

Figure 11. Computed mass flow rate non-uniformity index during the first 500 s of the simulation of the experiment of Figure 8, for the four bricks of the filter.

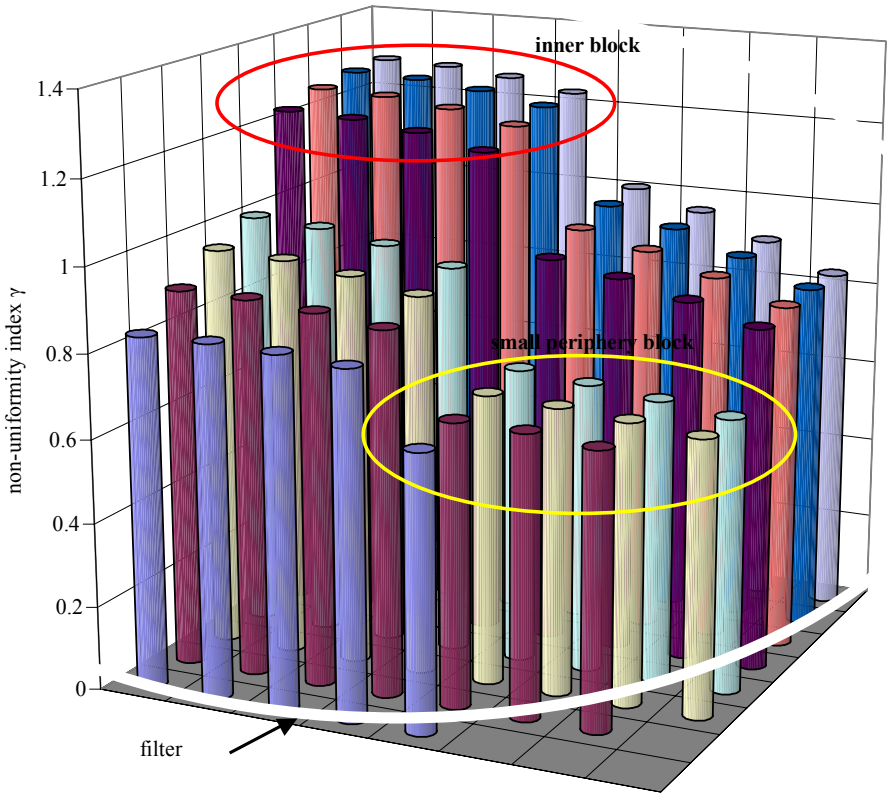

Figure 12. Computed percentage of the flow entering each sector of the 3-D model at t=300 s for the regeneration experiment of Fig.8.

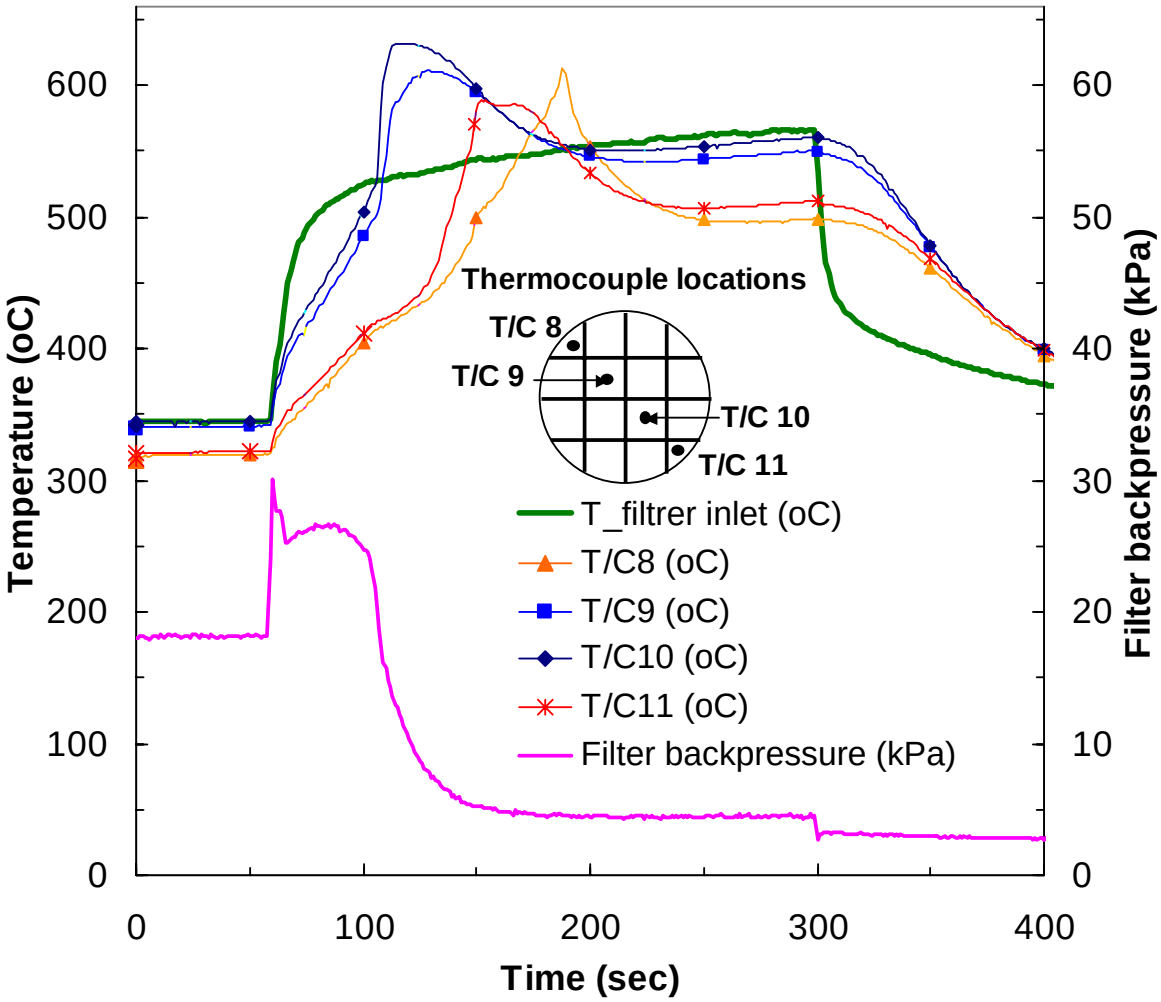

Figure 13 Test results of a medium flowrate regeneration scenario (52g/s). Measured temperatures along a filter diameter near channels exit together with filter backpressure are presented during regeneration at 4000rpm, 30Nm. Moderate filter loading (6g/l) have been accumulated with engine running at 3000rpm, 40Nm with 25ppm Ce-doped fuel.

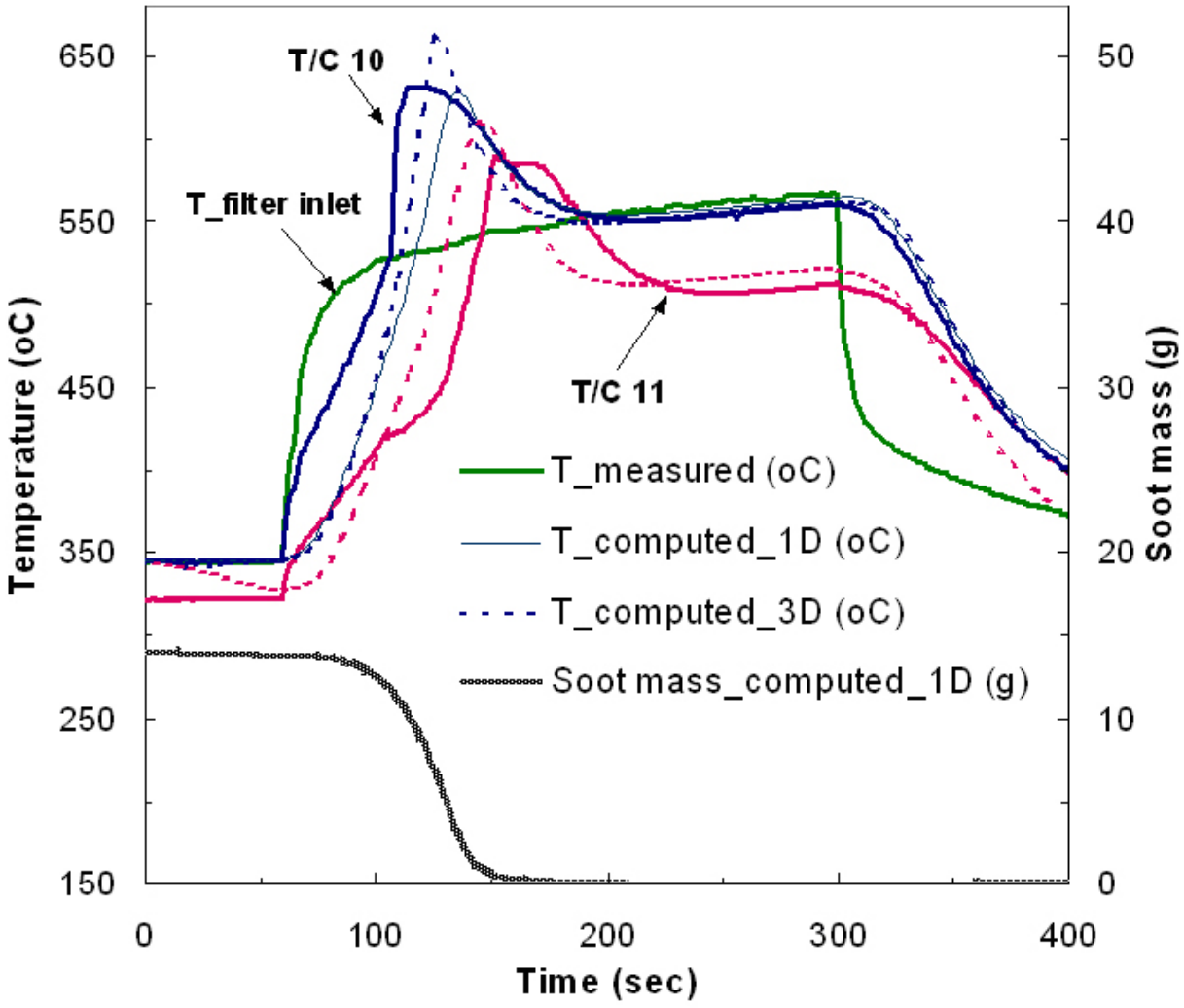

Figure 14 Computational simulation of the regeneration of Fig.13 by the 1-D and the 3-D codes. Predictions of measured temperatures by thermocouples T/C10 (filter central area) and T/C11 (near filter periphery) are presented for comparison. Predicted soot mass is also shown.

REFERENCES

1 O. Salvat, P. Marez, G. Belot, "Passenger Car Serial Application of a Particulate Filter System on a Common Rail Direct Injection Diesel Engine", *SAE paper 2000-01-0473*.

2 G. C. Koltsakis, A. M. Stamatelos, "Catalytic Automotive Exhaust Aftertreatment". *Prog. Energy Combust. Sci. Vol. 23, pp.1-39, 1997.*

3 C.D. Depcik: "Modeling Reacting Gases and Aftertreatment Devices for Internal Combustion Engines" *PhD Thesis, University of Michigan, 2003*

4 G. Pontikakis, A. Stamatelos, K. Bakasis and N. Aravas "3-D Catalytic Regeneration and Stress Modeling of Diesel Particulate Filters by ABAQUS FEM Software". *SAE paper 2002-01-1017*.

5 Bissett, E.; Shadman, F., "Thermal Regeneration of Diesel-Particulate Monolithic Filters" *AlChE J.* 1985, *31* (5), 753-765.

6 Bissett E., "Mathematical Model of the Thermal Regeneration of a Wall-Flow Monolith Diesel Particulate Filter" *Chem. Eng. Sci., 39, pp. 1232, 1984.*

7 G. C. Koltsakis, A. M. Stamatelos, "Modeling Thermal Regeneration of Diesel Particulate Traps" *AIChE Journal, Vol.42, No.6, 1662-1672, June 1996.*

8 G. C. Koltsakis, A. M. Stamatelos, "Modeling Catalytic Regeneration of Diesel Particulate Traps". *Industrial & Engineering Chemistry Research, 1996, (35), pp. 2-13.*

9 G. C. Koltsakis, A. M. Stamatelos, "Modes of Catalytic Regeneration in Diesel Particulate Filters" *Ind. Eng. Chem. Res. 1997, 36, 4155-4165*

10 G. A. Stratakis, G. N. Pontikakis and A. M. Stamatelos, "Experimental Validation of a Fuel Additive Assisted Regeneration Model in SiC Diesel Filters". *Proc. Instn. Mech. Engrs., Vol. 218, Part D: J. Automobile Engineering, (2004) 203-216*.

11 University of Thessaly / LTTE: "CATWALL Diesel Particulate Filter Modeling Software. *User's Manual". Version v4r3 Volos, September 2003*

12 G.Stratakis, "Experimental Investigation of Catalytic Soot Oxidation & Pressure Drop Characteristics in Wall-Flow Diesel Particulate Filters" *PhD Thesis, Mechanical Engineering Dept., University of Thessaly, January 2004.* (http://www.mie.uth.gr/labs/ltte/pubs/PhD_Stratakis.pdf)

13 O. Haralampous, G. Koltsakis, "Intra-layer temperature gradients during regeneration of diesel particulate Filters". *Chemical Engineering Science 57 (2002) 2345 – 2355*

14 H. Aoki, A. Asano, K. Kurazono, K. Kobashi and H. Sami., "Numerical Simulation Model for the regeneration Process of a Wall-Flow Monolith Diesel Particulate Filter". *SAE paper 930364*.

15 Miyairi, Y., Miwa, S., Abe, F., Xu, Z., & Nakasuji, Y. (2001)., "Numerical study on forced regeneration of wall-flow diesel particulate filter". *SAE paper, 2001-01-0912*.

16 Opris, C. N., & Johnson, J. H. (1998), "A two-dimensional computational model describing the flow and filtration characteristics of a ceramic diesel particulate trap". *SAE paper 980545*.

17 G.A. Stratakis and A.M. Stamatelos, "Flow distribution Effects in the Loading and Catalytic Regeneration of Wall-Flow Diesel Particulate Filters" *Proc Instn Mech Engrs Vol. 218 Part D: J Automobile Engineering (D2) 203-216 (2004)*

18 Gerd Gaiser, "Prediction of Pressure Drop in Diesel Particulate Filters Considering Ash Deposit and Partial Regenerations". SAE paper 2004-01-0158

19 ANSYS 5.7 User's Manual. "Guide to ANSYS User Programmable Features. Guide to Interfacing with ANSYS". *ANSYS Inc. Canonsburg, PA May 2001.*

20 S. C. Sorenson, Jacob W. Hoj, Per Stobbe, "Flow Characteristics of SiC Diesel Particulate Filter Materials". *SAE paper* 940236

21 S. Ebener, P. Florchinger, "Drukverlustmodel fuer keramische Dieselpartikelfilter" *Motortechnische Zeitscrift 2000, 61, 6, 414-422*

22 Frank P. Incropera and David P. DeWitt, "Fundamentals of Heat and Mass Transfer". *J.Wiley and Sons New York, 4th Ed. 1996.*

23 W.F. Stoecker, "Design of Thermal Systems" *3rd Edition, McGraw Hill Inc. New York 1989*.

24 G. Pontikakis, "Modeling, Reaction Schemes and Parameter Estimation in Catalytic Converters and Diesel Filters". *PhD Thesis, Mechanical Engineering Dept., University of Thessaly, Volos, June 2003*. (http://www.mie.uth.gr/labs/ltte/pubs/PhD_G_Pont.pdf)

25 University of Thessaly / LTTE: "ANSYS 5.7-CATWALL v4r3 Interfacing: 3D Modeling of Diesel Particulate Filters" *User's Manual. Version v4r3 Volos, December 2003*

26 G. A. Stratakis and A. M. Stamatelos, "Thermogravimetric Analysis of Soot Emitted by a Modern Engine Run on Catalyst-Doped Fuel". *Combustion and Flame 132 (2003) 157–169*